

# <sup>1</sup> Chapter 1

## <sup>2</sup> Diamond irradiation study

<sup>3</sup> The aim of the study in this chapter is to find the operational limitations of diamond  
<sup>4</sup> detectors for spectroscopy and tracking applications. The chapter contains the mea-  
<sup>5</sup> surement results of data taken with diamond sensors. First the measurement setup  
<sup>6</sup> is described in section 1.1. Then the measured particle spectra are shown in 1.2.  
<sup>7</sup> This is followed by a study of effects of the irradiation damage on the electrical signal  
<sup>8</sup> of the diamond detector. The last section shows the results of the measurements  
<sup>9</sup> of irradiated diamond samples at cryogenic temperatures. The studies compare the  
<sup>10</sup> experimentally acquired data with the theory from the previous chapter and define  
<sup>11</sup> limitations of the diamond detectors in terms of radiation and temperature.

<sup>12</sup> Diamond sensors are mainly used for two types of measurements: particle counting  
<sup>13</sup> and spectroscopy. The first type of measurements depends on the sensor efficiency –  
<sup>14</sup> its ability to detect all or at least a known percentage of incident particles. The energy  
<sup>15</sup> of the particles is not so important; what bears the information is the rate and the  
<sup>16</sup> spatial distribution. Here the particles do not necessarily stop in the bulk, but rather  
<sup>17</sup> continue their way. In spectroscopy, on the other hand, the particles stop within the  
<sup>18</sup> sensor, depositing all their energy. This energy is then measured by collecting the  
<sup>19</sup> freed charge carriers. The goal of the experiments described in this chapter is to:

- <sup>20</sup> 1. Quantify the efficiency of the sCVD diamond in counting mode,
- <sup>21</sup> 2. Quantify the degradation of the efficiency as a function of the received radiation  
dose,
- <sup>23</sup> 3. Quantify the macroscopic effects on charge carrier behaviour as a function of  
the received radiation dose and
- <sup>25</sup> 4. Define limitations for use in spectroscopy.

<sup>26</sup> The results discussed here show that there are several limitations for using diamond as  
<sup>27</sup> a radiation detector. All of them need to be taken into account when designing a new  
<sup>28</sup> measurement device. The irradiation study allows for an estimation of the lifetime of  
<sup>29</sup> the detector and a prediction of the longterm signal degradation as a function of the  
<sup>30</sup> received radiation dose. The result of the study is a correction factor, which can be

## 1.1. MEASUREMENT SETUP

---

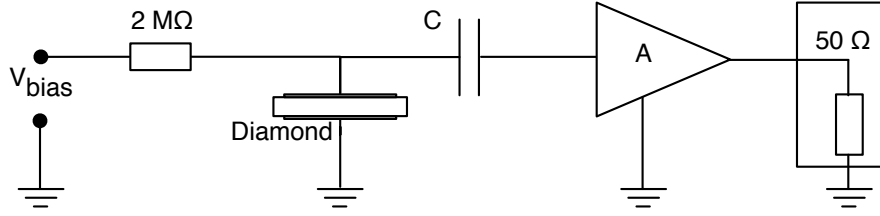


Figure 1.1: Diagram of a diamond detector readout chain.

<sup>31</sup> applied during data analysis to ensure that the analysis results are stable despite the  
<sup>32</sup> detector degradation.

### <sup>33</sup> 1.1 Measurement setup

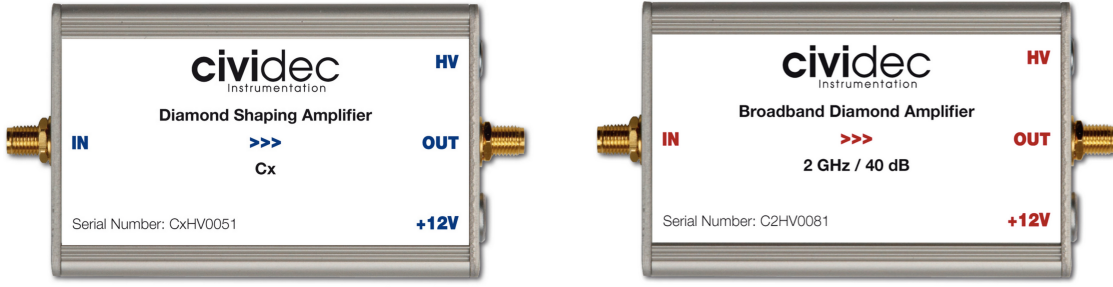
<sup>34</sup> The first step of designing a measurement setup is to define the measurement conditions,  
<sup>35</sup> such as the temperature, the type of radiation and its flux. The second step is  
<sup>36</sup> to ensure that the setup is insensitive to external electromagnetic interferences and  
<sup>37</sup> that it minimises electrical noise in the system. The setup needs to be calibrated  
<sup>38</sup> before use.

<sup>39</sup> Shielding has to be applied wherever possible. For instance, aluminium foil can  
<sup>40</sup> be wrapped around the exposed parts of the system to shield them from external  
<sup>41</sup> radio-frequency (RF) interferences. In addition, the sensors have to be covered to  
<sup>42</sup> prevent the exposure to light. The incident photons may deposit enough energy to  
<sup>43</sup> increase the leakage current of the detector, which produces unwanted results.

<sup>44</sup> The measurements using diamond that are explained in these chapters have been  
<sup>45</sup> carried out using several measurement setups, but they are all similar in terms of  
<sup>46</sup> the electrical signal chain. The measurement chain consists of three main parts: a  
<sup>47</sup> diamond sensor, a signal preamplifier and a readout device, as seen in figure 1.1. The  
<sup>48</sup> signals propagating along the analogue chain are fast – in the GHz bandwidth range –  
<sup>49</sup> and with low amplitudes – of the order of tens of  $\mu\text{V}$ . This gives rise to the importance  
<sup>50</sup> of RF shielding. Also, the connection between the carrier and the preamplifier has  
<sup>51</sup> to be as short as possible to avoid capacitive signal losses in the transmission line.  
<sup>52</sup> Finally, the system needs to be grounded properly.

#### <sup>53</sup> 1.1.1 Preamplifiers

<sup>54</sup> Two preamplifiers are used for the measurements, one sensitive to charge and the  
<sup>55</sup> other to current. *CIVIDEC Cx* (figure 1.2a) is a charge sensitive amplifier. Its high  
<sup>56</sup> SNR is achieved due to a low equivalent noise charge of  $300 \text{ e}^-$  with an additional  
<sup>57</sup>  $30 \text{ e}^-$  per each pF of the sensor capacitance. A reported gain of  $\sim 12 \text{ mV/fC}$  makes  
<sup>58</sup> it a good choice for spectroscopic measurements with diamond sensors. *CIVIDEC*  
<sup>59</sup> *C2* (figure 1.2b) is a fast current preamplifier with a 2 GHz bandwidth limit. It is  
<sup>60</sup> used for TCT measurements because of its fast response and a good SNR. Both are



(a) Cx charge sensitive preamplifier.

(b) C2 fast charge preamplifier.

Figure 1.2: Amplifiers used for the charge and current measurements.

61 embedded in an RF-tight aluminium box to reduce the noise pickup. Both have an  
62 AC coupled input and an output with a  $50\ \Omega$  termination.

63 A 2 GHz bandwidth limit defines the minimum rising time equal to  $t_r \simeq \frac{0.34}{BW} =$   
64  $\frac{0.34}{2 \times 10^9} = 170\ ps$ , therefore the system with a CIVIDEC C2 amplifier is capable of  
65 measuring pulses with a minimum FWHM  $\simeq 170\ ps$ . The initial peak in the  $\alpha$  pulse  
66 has a lower FWHM; for example, if a charge carrier travelling through the bulk takes  
67  $t_1 \sim 6\ ns$  to reach the electrode on the opposite side ( $d_1 \sim 500\ \mu m$ ), the carrier with  
68 the opposite charge and a shorter path to the closer electrode – max.  $d_2 \sim 10\ \mu m$  –  
69 only takes  $t_2 \sim \frac{d_2}{d_1} t_1 = 120\ ps$ . A drift time this short induces a current pulse that is  
70 too narrow for the system to observe.

## 71 Calibration

72 The amplifiers have to be calibrated before use to determine their gain. Both are  
73 calibrated using a square signal generator with a known amplitude step of  $U_{in} =$   
74  $(252 \pm 5)\ mV$ . A 2 GHz oscilloscope with a 10 GS/s sampling rate is used to carry  
75 out the calibration.

76 **Cx charge sensitive amplifier** calibration necessitates an injection of a well known  
77 charge. Therefore the signal from a pulse generator is routed through a capacitor with  
78 a calibration capacitance  $C_{cal} = (0.717 \pm 0.014)\ pF$  and then to the input of the am-  
79 plifier. The pulse area behind the capacitor is  $a_{cal} = (5.0 \pm 0.5)\ pVs$ , with the signal  
80 amplitude on the output amounting to  $U_{Cx} = (1.95 \pm 0.05)\ V$ . The input voltage step  
81 combined with the calibration capacitance yields a calibration charge

$$Q_{cal} = C_{cal} \cdot U_{in} = (181 \pm 5)\ fC. \quad (1.1)$$

82 The gain of the Cx amplifier when comparing the integrated input charge to the  
83 output amplitude is

$$A_{Cx}^Q = \frac{U_{Cx}}{Q_{cal}} = (9.3 \pm 0.4)\ mV/fC \quad (1.2)$$

## 1.1. MEASUREMENT SETUP

---

84 whereas the factor between the area of the input current pulse and the output am-  
 85 plitude is

$$A_{Cx}^a = \frac{U_{Cx}}{a_{cal}} = (390 \pm 40) \text{ mV/pVs.} \quad (1.3)$$

86 The area-based amplification factor  $A_{Cx}^a$  can be used as an estimate for the integrated  
 87 charge of a current pulse. However, it has a higher uncertainty ( $\sim 10\%$ ) than  
 88 the amplitude-based factor  $A_{Cx}^Q$  ( $\sim 4\%$ ) due to the measurement limitations of the  
 89 oscilloscope.

90 **C2 current amplifier** calibration only requires the measurement of the amplitude  
 91 gain. To keep the output signal amplitude within the  $\pm 1$  V linear range of the  
 92 amplifier, the input signal amplitude has to be minimised. The signal from the  
 93 generator is therefore routed through a 36 dB attenuator to decrease its amplitude to  
 94  $U_{inAtt} = (3.95 \pm 0.05)$  mV. Two amplifiers with different gains have been measured,  
 95 because both are used for the measurements. The output of the first amplifier amounts  
 96 to  $U_{C2-1} = (860 \pm 5)$  mV. This yields the amplification gain

$$A_{C2-1} = \frac{U_{inAtt}}{U_{C2-1}} = (217 \pm 3). \quad (1.4)$$

97 The second amplifier has the output equal to  $U_{C2-2} = (632 \pm 5)$  mV with the resulting  
 98 gain of  $A_{C2-2} = (152 \pm 3)$ .

### 99 1.1.2 Diamond samples

100 Detector-grade diamonds are very difficult to produce. The major challenge is to  
 101 ensure a high enough purity of the lattice. The sensor samples used for these studies  
 102 have been acquired from Element Six (E6) [2]. They all have the same standard  
 103 dimensions. sCVD diamonds with dimensions  $4.7 \times 4.7 \text{ mm}^2$  are already sufficiently  
 104 large for most of the beam monitoring applications and still affordable. One sample  
 105 with dimensions of  $5.6 \times 5.3 \text{ mm}^2$  produced by IIa Singapore [3] has also been char-  
 106 acterised at CERN [19]. The target thickness for all samples is 500  $\mu\text{m}$ . Diamonds  
 107 this thick yield a high enough signal-to-noise ratio for MIPs to be measured by the  
 108 available electronics. Table 1.1 shows all the samples used for this study. Two of  
 109 them are measured before and after irradiation and then compared. Irradiation doses  
 110 for damaging the material need to be high – above  $10^{12}$  particles per  $\text{cm}^2$  to be able  
 111 to observe a significant change in behaviour of a diamond sensor.

Name	Type	Producer	Dimensions [ $\text{mm}^2$ ]	Thickness [ $\mu\text{m}$ ]	Electrode	Irradiated
S37	sCVD	E6	$4.7 \times 4.7$	548	Cr/Au	no
S50	sCVD	E6	$4.7 \times 4.7$	537	Cr/Au	no
S52	sCVD	DDL	$4.7 \times 4.7$	515	DLC/Pt/Au	$3.63 \times 10^{14} \frac{\pi}{\text{cm}^2}$
S79	sCVD	E6	$4.7 \times 4.7$	529	Cr/Au	$1 \times 10^{14} \frac{\pi}{\text{cm}^2}$
ELSC	sCVD	E6	$4.7 \times 4.7$	491	Cr/Au	no
1scdhq	sCVD	IIa	$5.6 \times 5.3$	460	Cr/Au	no

114 Table 1.1: Diamond sensor samples used.

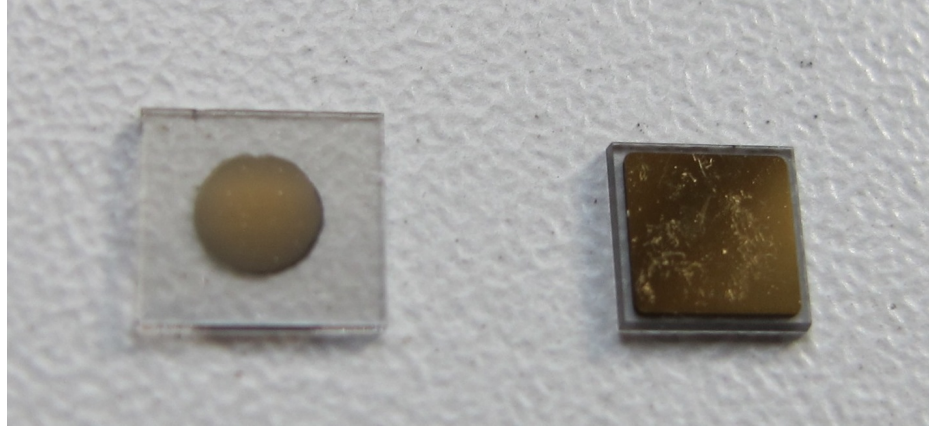


Figure 1.3: Two scCVD diamond samples: A IIa 1scdhq (left) and an E6 S37 (right).

The diamond samples have quoted impurity densities of  $\leq 2 \times 10^{14} \text{ cm}^{-3}$  and nitrogen incorporation of  $\leq 10^{-9}$ . The electrodes were added by various companies and institutes. For instance, S52 was metallised by a company DDL (now defunct) while the Physics Department of the University of Firenze, Italy metallised the S79. There are also several techniques for producing the electrodes. The DDL contacts consist of three layers: DLC (diamond-like carbon)/Pt/Au with 4/10/200 nm thicknesses, respectively. The metallisation for S79, on the other hand, is made up of Cr/Au with a total thickness of  $\sim 400$  nm. The area coverage also differs from sample to sample. Diamonds must not be metallised until the very edge as the proximity of contacts with a high potential may lead to sparking. However, the areas not covered by the metallisation are less efficient because the fringe fields at the edges are not as strong as in between the electrodes. This effectively reduces the sensitive area of the sensors. In the diamonds used here the effective area is anywhere from  $9 \text{ mm}^2$  to  $18 \text{ mm}^2$ . The leakage current is below 1 nA, but increases for the irradiated samples. The capacitance is of the order of  $(2.0 \pm 0.3)$  pF.

### 1.1.3 Readout devices

Electrical signals in diamond detectors are in the GHz frequency range. To preserve the information in the signals, the readout device with a high bandwidth limit must be used. For instance, a 250 MHz limit is enough for the spectroscopic measurements with the Cx charge amplifier, but might be insufficient for the current measurements with the C2 amplifier.

Two devices are used take data shown in this chapter. The first choice is a 2 GHz LeCroy WaveRunner 204MXi-A. This specific model has a sufficiently high bandwidth limit for the fast current preamplifier signals. It offers a reliable solution for analogue signal readout of limited amounts of data. However, its slow acquisition speed is a bottleneck in a test beam experiment. Its initial 100 Hz readout rate decreases to a mere 20 Hz within 20 minutes, because every single trigger is saved as a separate file and the Windows operating system is not capable of handling 10000+ files in a single

## 1.1. MEASUREMENT SETUP

---

143 directory easily. This is why it has been exchanged with a DRS4 [1], an analogue  
144 readout device developed by PSI, Switzerland. This compact device is capable of  
145 recording up to four waveforms at a time at a steady rate of up to 500 Hz. Its  
146 700 MHz bandwidth limitation is sufficient for the signal from the charge amplifier.

### 147 1.1.4 Setup for the $\beta$ detection efficiency study

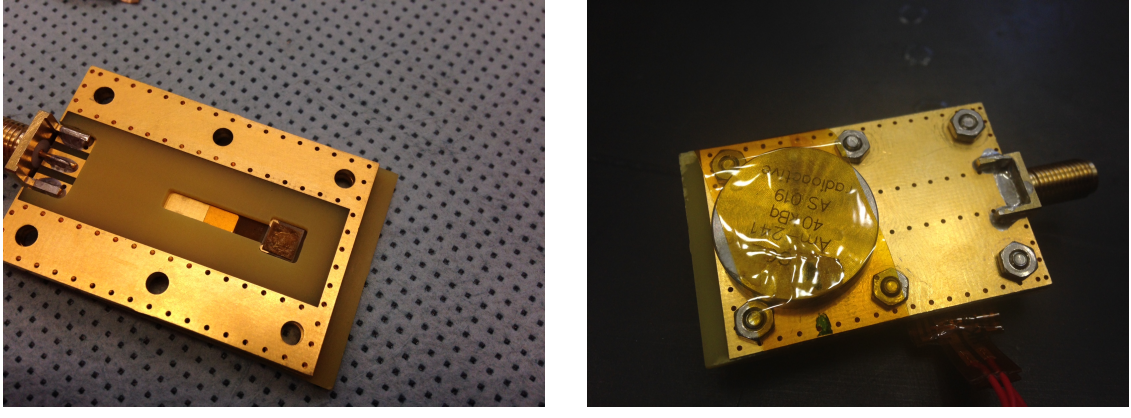
148 The efficiency study of the diamond sensors has been carried out at CERN in the  
149 North Hall test beam facility. There a straight high-energy particle beam of 120 GeV  $\pi$   
150 is provided to the users to calibrate their detectors. The beam has a transverse spread  
151 of  $\sigma = 10$  mm in both axes. The particle rate is of the order of  $10^4 \pi \text{ cm}^{-2} \text{ s}^{-1}$ . A  
152 diamond sensor embedded in a printed circuit board (PCB) carrier has been placed  
153 in the beam spot perpendicular to the beam and connected via an SMA connector  
154 directly to a charge amplifier. The amplified signal is read out using a LeCroy oscillo-  
155 scope and a DRS4 analogue readout system. A computer is used as a controller and  
156 data storage for the readout device. A beam telescope is used as a reference detector.  
157 It is a device that helps to cross-check the measurements of the devices under test  
158 (DUTs) and to carry out spatially resolved studies on the DUTs. It consists of several  
159 pixellated sensor planes placed in series, which can track a particle's trajectory with  
160 a precision of a few  $\mu\text{m}$ . The sensor planes are positioned in front of the DUT and  
161 behind it. Then the beam telescope acts as a trigger system – it triggers the readout  
162 of both the telescope data and DUT data when both the planes in front and behind  
163 the DUT record a hit by an incident particle. A particle detected by all the planes  
164 within the DUT window and the DUT itself counts towards its efficiency whereas a  
165 hit missed by the DUT means that the DUT is not 100 % efficient. To discard the  
166 hits that miss the DUT completely, a region of interest (ROI) can be chosen in the  
167 beam telescope planes. The equation for calculating the sensor efficiency is therefore

$$\epsilon = \frac{N_{\text{DUT}} \wedge N_{\text{telescope}}}{N_{\text{telescope}}} \quad (1.5)$$

168 for an ROI smaller than the sensitive region of the diamond.

### 169 1.1.5 Room temperature $\alpha$ -TCT setup

170 This TCT study is a follow-up of an extensive diamond TCT study at cryogenic  
171 temperatures [13]. The room-temperature TCT measurements have been carried  
172 out in the laboratory. The setup consists of a diamond sensor embedded in a PCB  
173 carrier, a current amplifier and an oscilloscope. To measure  $\alpha$  particles, their energy  
174 loss during their trajectory has to be minimised. Therefore the diamond is placed  
175 inside a vacuum chamber. The chamber is a steel tube with a diameter of 5 cm.  
176 On one side it is connected to a vacuum pump via a steel hose. A feedthrough with  
177 an SMA connector is placed on the other side. A CIVIDEC C2 current amplifier is  
178 connected directly onto the feedthrough. The amplified output is connected to the  
179 oscilloscope via an SMA cable. An  $^{241}\text{Am}$  source with a diameter of 2 cm and a



(a) PCB carrier with an embedded diamond sample.  
 (b) Radioactive source over the carrier.

Figure 1.4: Positioning of the  $\alpha$ -source on top of the sensor carrier.

height of 0.5 cm is fixed onto the sensor carrier (figure 1.4a, figure 1.4b). Then the carrier is inserted in the chamber and fixed in place using an air-tight clamp. The pump can then be switched on. It is capable of providing the inside pressure as low as  $10^{-4}$  mbar after approximately one hour of operation.

### 1.1.6 Cryogenic $\alpha$ -TCT setup

The experiment at cryogenic temperatures has been carried out at the Central Cryogenic Laboratory at CERN. The room-temperature TCT setup has to be modified to allow for measurements at temperatures as low as 2 K. It consists of three parts:

1. a cryostat – a thermally insulated cylinder containing liquid helium,
2. an inlet – an air-tight mechanical tube with valves and feedthroughs at the top that is lowered in the liquid helium and
3. the diamond sample embedded in a PCB carrier with a fitted temperature sensor, a heater and cables leading to the feedthroughs.

The setup is described in detail in [13].

When the diamond sample is placed in the PCB carrier and the  $^{241}\text{Am}$  source is in place, the inlet is sealed and lowered in the empty cryostat. Then the inside volume of the inlet is evacuated down to  $10^{-5}$  mbar while the liquid helium is flowing into the cryostat. To improve the thermal contact between the diamond and the coolant, a small amount of helium gas is added inside the evacuated inlet, setting the vacuum to around  $10^{-3}$  mbar. This value changes with time, because the gas condenses on the walls of the inlet, reducing the number of floating particles. For this reason the helium gas has to be added on an irregular basis. Every addition causes a significant undershoot of the sample temperature, which has to be corrected for using

## 1.2. CHARGED PARTICLE PULSES AND SPECTRA

---

203 a heater placed on the back of the PCB carrier. Also, the added gas deteriorates the  
204 vacuum inside the inlet. Furthermore, at approximately 60 K the helium gas has to  
205 be evacuated from the inlet to avoid a potential explosion due to the expansion of  
206 the gas with temperature.

207 When the sample is cooled to 4.2 K, the minimum temperature achievable by  
208 means of liquid helium without over-pressurising it, the measurements can begin. A  
209 temperature sensor placed on the back of the PCB carrier is used to measure the  
210 temperature of the sample. After every temperature data point, the current through  
211 the heater placed in the PCB next to the diamond sample is increased, increasing the  
212 sample. The initial temperature time constant of the order of tenths of seconds at low  
213 temperatures increases with temperature. Even more so when helium is evacuated  
214 from the inlet at 60 K, removing the thermal bridge between the wall of the inlet and  
215 the diamond sample. At the room temperature (RT), the time constant is already of  
216 the order of minutes.

## 217 1.2 Charged particle pulses and spectra

218 In previous chapter the ionisation profiles for different types of radiation were dis-  
219 cussed.  $\beta$  radiation induces a triangular electric pulse whereas  $\alpha$  radiation induces  
220 a rectangular one. However, their amplitude, width and rise/fall time depend heav-  
221 ily on the type of interaction with the diamond, the purity of the diamond and the  
222 bandwidth of the amplifier and the oscilloscope. This section shows the signal pulses  
223 of  $\alpha$ ,  $\beta$  and  $\gamma$  radiation with their respective energy distributions for the case of a  
224 diamond detector.

225 Figure 1.5 shows a set of pulses and an averaged waveform for 5.5 MeV  $\alpha$ , 2.3 MeV  
226  $\beta$  and 1.3 MeV  $\gamma$  radiation using an  $^{241}\text{Am}$ , a  $^{90}\text{Sr}$  and a  $^{60}\text{Co}$  source, respectively.  
227 The particles are measured with the non-irradiated sCVD diamond S37.  $\alpha$  particles  
228 always produce the same signal pulse, but with a high noise RMS. The averaging  
229 suppresses the noise while retaining most the information. It does, however, smear  
230 the rising and falling edge, increasing the rising and falling time. The  $t_r$  is now of  
231 the order of 0.5 ns. Both  $\beta$  and  $\gamma$  pulses look similar - triangular and with a wide  
232 range of amplitudes. Here the pulse count is low, so the pulses with a high amplitude  
233 are not recorded. A trigger would need to be set very high to “catch” them with the  
234 oscilloscope.

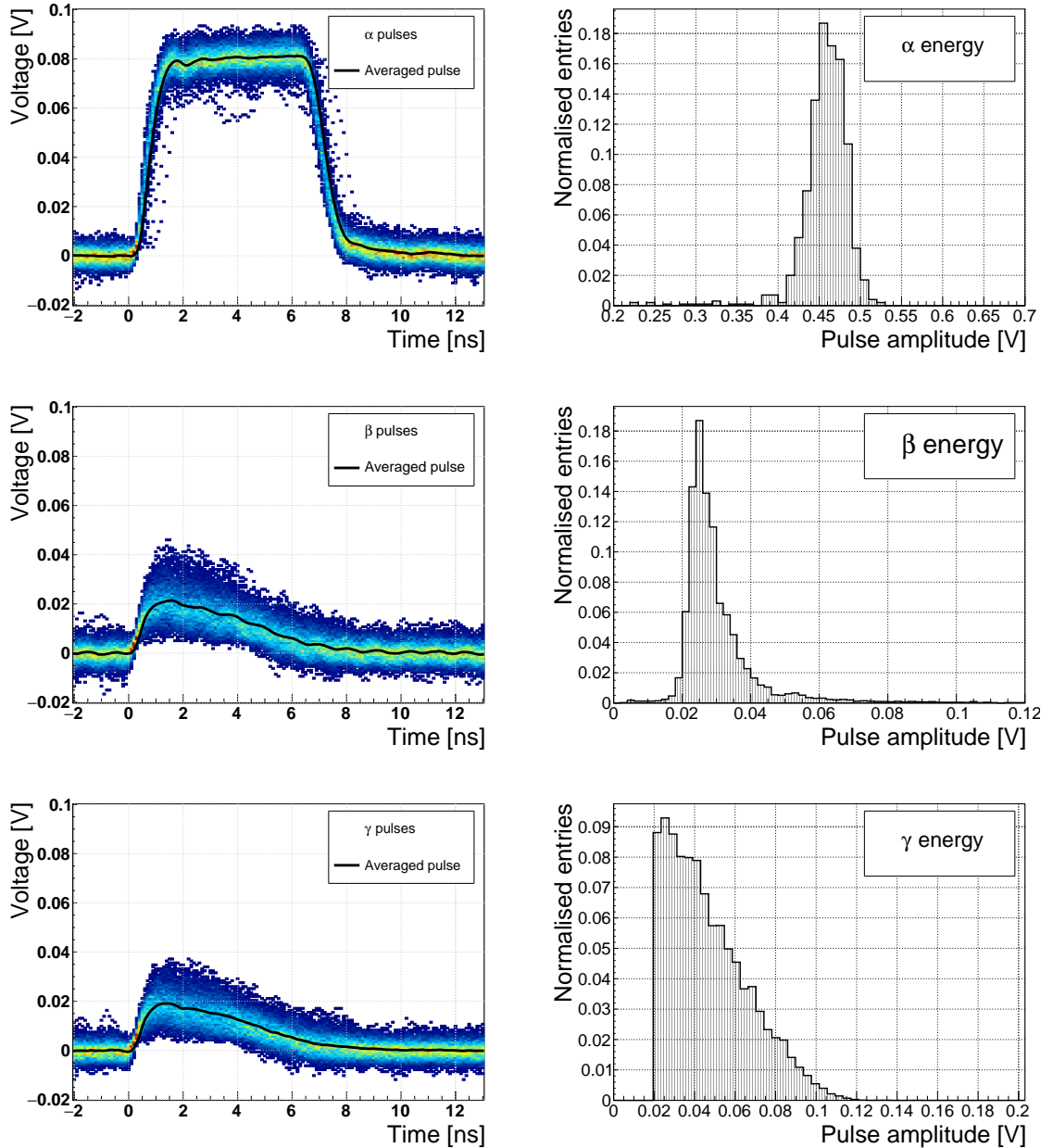


Figure 1.5: Superimposed and averaged pulses (left figures, current amplifier) and distributions of deposited energy (right figures, charge amplifier) for three types of radiation. Note the scale on the X axis of the distributions.

<sup>235</sup> **1.3 Radiation limitations**

<sup>236</sup> This section quantifies the decrease in charge collection efficiency as well as the effects  
<sup>237</sup> on long-term measurement stability in irradiated sCVD diamonds.

<sup>238</sup> **1.3.1 Irradiation study**

<sup>239</sup> This subsection contains a study of the effects of 300 MeV pion ( $\pi$ ) irradiation  
<sup>240</sup> on the charge collection efficiency of sCVD diamond detectors. To carry out this  
<sup>241</sup> study, two diamond samples were irradiated to doses of  $1 \times 10^{14} \pi \text{ cm}^{-2}$  (S79) and to  
<sup>242</sup>  $3.63 \times 10^{14} \pi \text{ cm}^{-2}$  (S52). A test beam campaign was carried out to observe the charge  
<sup>243</sup> collection efficiency at different bias voltage settings. The efficiency values acquired  
<sup>244</sup> are used to determine the effective drop in efficiency as a function of the received  
<sup>245</sup> radiation dose. This is to test if the collected charge  $Q$  is inversely proportional to  
<sup>246</sup> the received dose  $\Phi$ . A procedure defined by a collaboration researching diamond be-  
<sup>247</sup> haviour RD42 has been applied to the measured values to extract the damage factor.  
<sup>248</sup> The following subsection contains measurements and results of a long-term stability  
<sup>249</sup> study using  $\alpha$  and  $\beta$  particles. In particular, the charge collection efficiency with  $\beta$   
<sup>250</sup> and  $\alpha$  radiation as a function of time is measured. To investigate this effect on the  
<sup>251</sup> scale of charge carriers, the change of TCT (transient current technique) pulses with  
<sup>252</sup> time is observed. Finally, a procedure that improves the pulse shape and with it the  
<sup>253</sup> charge collection is proposed.

<sup>254</sup> **Irradiation with a 300 MeV  $\pi$  beam**

<sup>255</sup> The samples were irradiated at the Paul Scherrer Institute (PSI) [4] by means of a  
<sup>256</sup> beam of pions with an energy of 300 MeV (kinetic energy 191.31 MeV) and with a flux  
<sup>257</sup> of up to  $1.5 \times 10^{14} \pi \text{ cm}^{-2}$  per day. The system has a 10 % uncertainty on the beam  
<sup>258</sup> energy. Looking at the pion damage curve in figure ??,  $\pi_{300 \text{ MeV}}$  point ( 191 MeV  
<sup>259</sup> kinetic energy) sits on a steep section of the DPA curve. This means that a deviation  
<sup>260</sup> in beam energy can have a significant effect on the damage in the sensor. In addition,  
<sup>261</sup> their quoted uncertainty on the measurement of the delivered dose is  $\pm 20 \%$ .

<sup>262</sup> Two diamond samples, S52 and S79, were put in the  $\pi_{300 \text{ MeV}}$  beam in the 2014  
<sup>263</sup> PSI irradiation campaign; S52 to  $(1 \pm 0.21) \times 10^{14} \pi \text{ cm}^{-2}$  and S79 to  $(3.63 \pm 0.77) \times$   
<sup>264</sup>  $10^{14} \pi \text{ cm}^{-2}$ . During the process, the gold electrodes got slightly activated, but the  
<sup>265</sup> activation decayed in two weeks.

<sup>266</sup> **300 MeV  $\pi$  radiation damage factor**

<sup>267</sup> Three diamonds – non-irradiated S37 and irradiated S52 and S79 – were tested in a  
<sup>268</sup>  $\pi_{120 \text{ GeV}}$  test beam in the SPS North Experimental Area at CERN [8] before and after  
<sup>269</sup> irradiation. The goal was to estimate the charge collection efficiency and charge col-  
<sup>270</sup> lection distance as a function of irradiation dose. The samples were primed (pumped)  
<sup>271</sup> prior to data taking using a  ${}^{90}\text{Sr}$  radioactive source. The data were then taken at

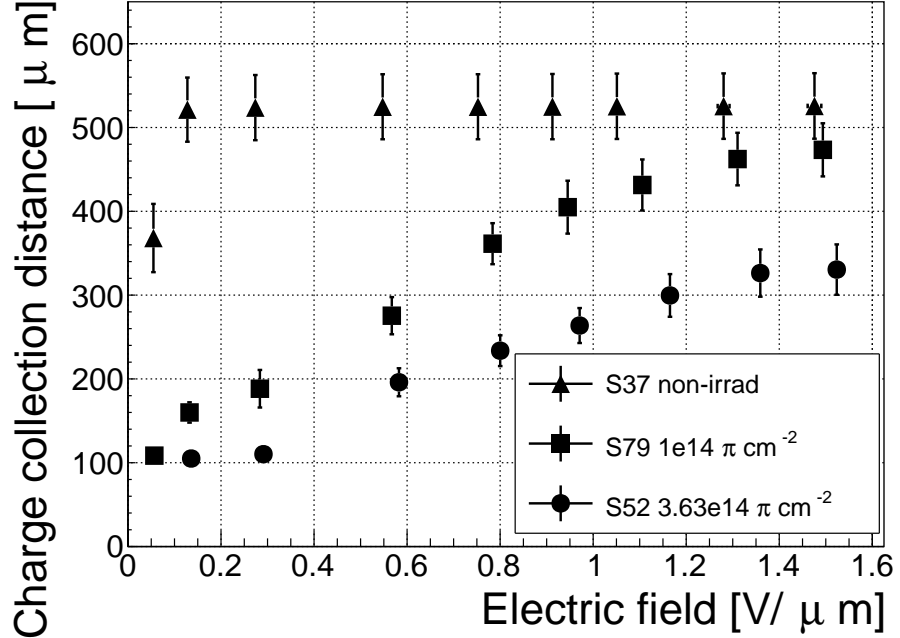


Figure 1.6: The figure shows the CCD for S37, S79 and S52 at a range of bias voltage settings.

a range of bias voltages ranging from 30 V to 900 V, yielding between 0.06 V/μm and 1.8 V/μm electrical field in the bulk. Every data point contained approximately  $5 \times 10^4$  measured particles. The charge deposited by the particles was measured using a CIVIDEC Cx charge preamplifier.

As expected, the integrated amplitude spectrum is a Landau distribution. Its most probable value (MPV) is used to calculate the most probable collected charge  $Q_i$ :

$$Q_i [e^-] = \frac{1}{1.6 \times 10^{-19}} Q_i [C] = 6241 \cdot Q_i [fC] = 6241 \cdot \frac{MPV [mV]}{A [\frac{mV}{fC}]}, \quad (1.6)$$

where  $A = 9.3$  mV/fC is the preamplifier gain factor and  $1 e^- = 1.6 \times 10^{-19} C$ .

The CCD for the three measured samples at a bias voltages ranging from 0.2–1.6 V  $\mu\text{m}^{-1}$  calculated using equation ?? is shown in figure 1.6. S37 exhibits a full collection distance already at 0.4 V  $\mu\text{m}^{-1}$  whereas the irradiated samples have a more gentle increase of CCD with increasing bias voltage. It is evident that at 1 V  $\mu\text{m}^{-1}$  the maximum CCD has not been reached in the case of S79 and S52. Nevertheless, to compare the measured data point with those provided by RD42, the CCD at 1 V  $\mu\text{m}^{-1}$  has to be taken.

The data points with the maximum CCD obtained in the test beam measurements are plotted against received radiation dose in figure 1.7. Equation ?? is fitted to the data points and a damage factor  $k_\lambda = (4.4 \pm 1.2) \times 10^{-18} \mu\text{m}^{-1} \text{cm}^{-2}$  is obtained. The value is for a factor of two higher than the damage factor obtained by RD42. This

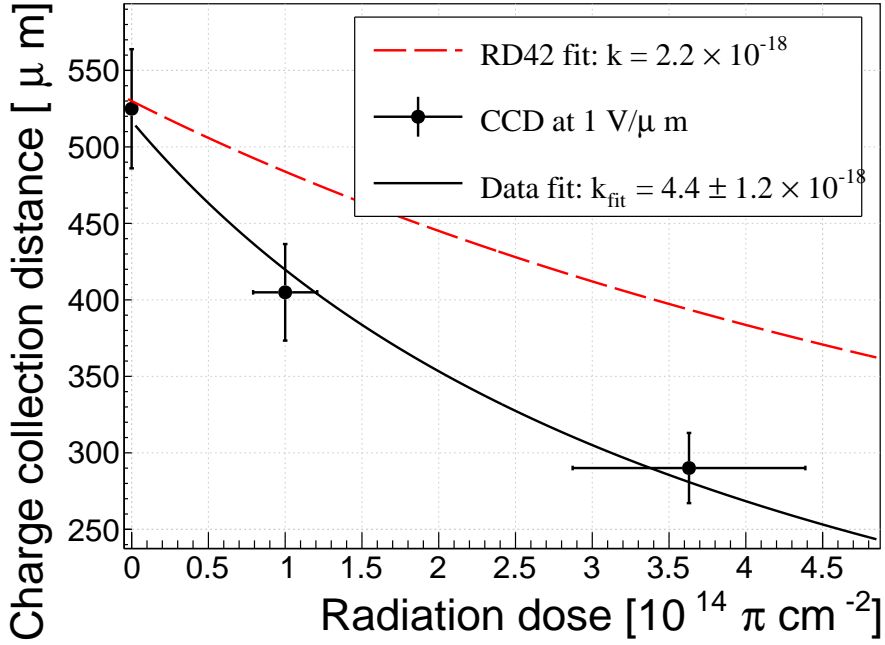


Figure 1.7: The charge collection distance at 1 V/ $\mu\text{m}$  bias voltage for the three diamond samples is plotted as a function of the received radiation dose. It is compared to the RD42 data for pion irradiation. The data points are about 15–25 % lower than expected from the RD42 data [17].

291 could be due to an insufficient priming time ahead of the measurement. In addition,  
 292 the diamond samples have not been polished and re-metallised after irradiation, as  
 293 is the case for the RD42. Also, with only two samples measured, the statistical  
 294 uncertainty is high. Nevertheless, it can be concluded that the 300 MeV pions damage  
 295 the diamond bulk significantly more than the 24 GeV protons.

### 296 1.3.2 Long-term measurement stability

297 An important requirement for particle detectors is a stable performance over long  
 298 periods of time. For instance, the charge collection for a defined radiation type and  
 299 quantity must not change over time or has to change in a predicted way. The stability  
 300 of diamond detectors depends on many factors: material purity, polishing process,  
 301 electrode material, irradiation damage etc. The aim is to study the behaviour of  
 302 diamond under controlled conditions, with the goal to understand its limitations.  
 303 One of these limitations is the received radiation dose as it can affect the long-term  
 304 stability of the sensor during operation.

305 The three diamond samples (S37, S79 and S52) have been exposed to two different  
 306 types of ionising radiation for a longer period to see if their behaviour changes over  
 307 time. Two parameters have been observed in particular:

- 308 1. Charge collection of  $\beta$  particles and

309        2. Charge collection and ionisation profile of  $\alpha$  particles.

310         **$\beta$  long-term stability**

311        The diamond samples have undergone a long-term stability test at room temperature  
312        using  $\beta$  radiation. This has been done using a  $^{90}\text{Sr}$  source emitting  $\sim 2$  MeV electrons  
313        at a rate of approximately  $10^4 \text{ e}^- \text{ cm}^{-2}$ . To simulate the initial conditions in HEP  
314        experiments, the sensors must not be primed before starting the measurements. The  
315        measurement setup consists of a diamond sample (S37, S52 or S79) with the CIVIDEC  
316        Cx spectroscopic amplifier, a silicon diode with a CIVIDEC C6 amplifier for triggering  
317        and a  $^{90}\text{Sr}$  source on top. A particle emitted by the source traverses the sensor bulk  
318        and hits the silicon diode, triggering the analogue signal readout. The source is  
319        left on the top for the course of the experiment. The measurements, however, are  
320        taken at discrete times. For every data point, approximately  $10^4$  triggers have to be  
321        recorded. The offline analysis of the recorded signal pulse amplitudes yields a Landau  
322        distribution for every data point. The current charge collection relative to the initial  
323        charge collection for every sample is plotted as a function of the received  $\beta$  dose in  
324        figure 1.8. It shows that, for the irradiated samples, the charge collection efficiency  
325        improves when the diamond sensor is primed with a  $\beta$  source. The effect is negligible  
326        for the non-irradiated high-quality S37. Both relative increases are significant – 22 %  
327        for S79 and 55 % for S52. At a received dose of approximately  $4 \times 10^6$  particles the  
328        charge collection is stabilised. At that point S79 achieves close to a full efficiency (in  
329        absolute values – not shown) whereas S52 reaches approximately 50 %.

330        The  $\sim 2.28$  MeV electrons emitted by this source are not MIPs; their charge depo-  
331        sition is higher than that of an electron MIP, according to the Bethe-Bloch distribu-  
332        tion [7]. Nevertheless, for the purpose of these measurements this energy is adequate  
333        since only the relative change in charge collection is of interest.

334        To sum up, diamond provides a stable measurement of the  $\beta$  radiation detection  
335        after reaching a stable state. Even if damaged by radiation, it reaches a stable charge  
336        collection at a received dose of  $\sim 4 \times 10^6$  MIPs. Its efficiency decreases with a high  
337        irradiation dose. However, the decrease can be accounted for if the damage factor  
338        and the rate and energy of the particles are known.  $\gamma$  radiation has a similar impact  
339        on the diamond as the  $\beta$ . The incident photons, if they interact with the diamond,  
340        prime the bulk, increasing the charge collection efficiency. The difference, however,  
341        is that the interaction probability (cross-section) is lower for gammas [18, 10].

342         **$\alpha$  long-term stability**

343        This part discusses the stability of irradiated diamond sensors during  $\alpha$  measurements.  
344        An  $^{241}\text{Am}$  source has been used, emitting  $\alpha$  particles with a mean energy of 5.5 MeV.  
345        They affect the diamond differently than when subjected to  $\beta$  radiation. This is due  
346        to the point-like charge carrier creation; an  $\alpha$  particle penetrates the bulk and stops  
347        at a depth of  $\sim 14 \mu\text{m}$  (for a 5.5 MeV particle). The deposited energy on its path

### 1.3. RADIATION LIMITATIONS

---

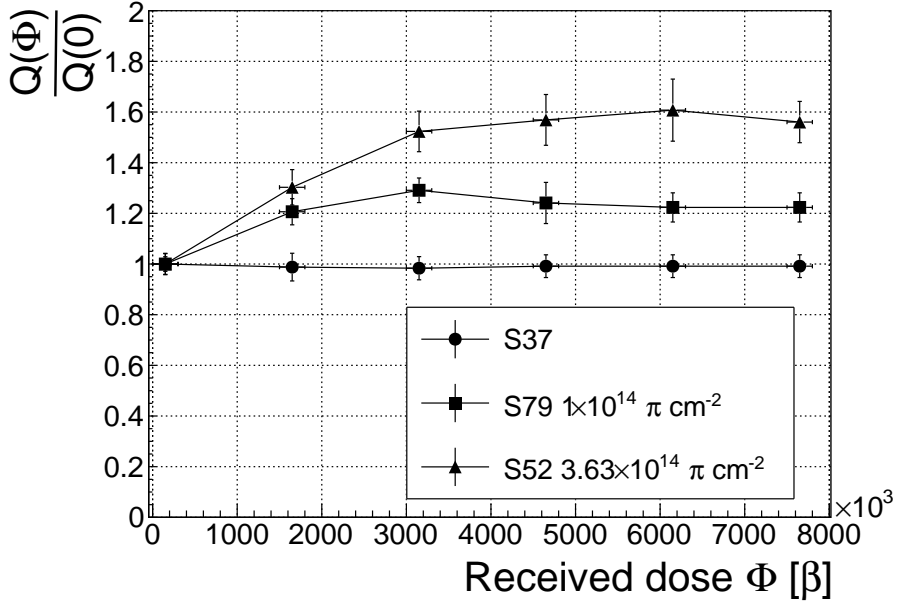


Figure 1.8: Relative increase of charge collection over time due to priming with the  $^{90}\text{Sr}$  radioactive source. The charge collection for the non-irradiated S37 stays constant. The bias voltage for this measurement is 1 V/ $\mu\text{m}$ .

<sup>348</sup> produces  $4 \times 10^5$  e-h pairs according to equation 1.7:

$$n_{\text{e-h}} = \frac{E}{E_{\text{e-h}}} \quad (1.7)$$

<sup>349</sup> where  $E$  is the deposited energy of the particle and  $E_{\text{e-h}}$  is the energy required to  
<sup>350</sup> create an electron-hole pair. The deposited energy and as a consequence the collected  
<sup>351</sup> charge for a MIP is significantly lower in comparison. According to equation 1.8 a  
<sup>352</sup> MIP produces  $18 \times 10^3$  e-h pairs in a 500  $\mu\text{m}$  thick diamond:

$$n_{\text{e-h}} = d \cdot E_{\text{avg}}, \quad (1.8)$$

<sup>353</sup> where  $d$  is the thickness of the sensor and  $E_{\text{avg}}$  is the average number of e-h pairs  
<sup>354</sup> created per micrometer. Thus the collected charge of a 5.5 MeV  $\alpha$  is for a factor  
<sup>355</sup> of 22 higher. In addition, the energy is deposited in a small volume – 14  $\mu\text{m}$  in  
<sup>356</sup> depth and  $\sim 20$  nm radially [13]. This dense distribution of charge carriers affects  
<sup>357</sup> their behaviour at the start of the drift. Furthermore, carriers of only one polarity  
<sup>358</sup> drift through the sensor while those of the opposite polarity almost instantly reach  
<sup>359</sup> the adjacent electrode. Taking into consideration that the diamond bulk has been  
<sup>360</sup> damaged by irradiation, these phenomena combined might have an effect on the  
<sup>361</sup> operation of the detector.

<sup>362</sup> To test the stability of the diamond during  $\alpha$  measurements, the samples have  
<sup>363</sup> been biased at +500 V and exposed to up to 8000  $\alpha$  hits while measuring their charge

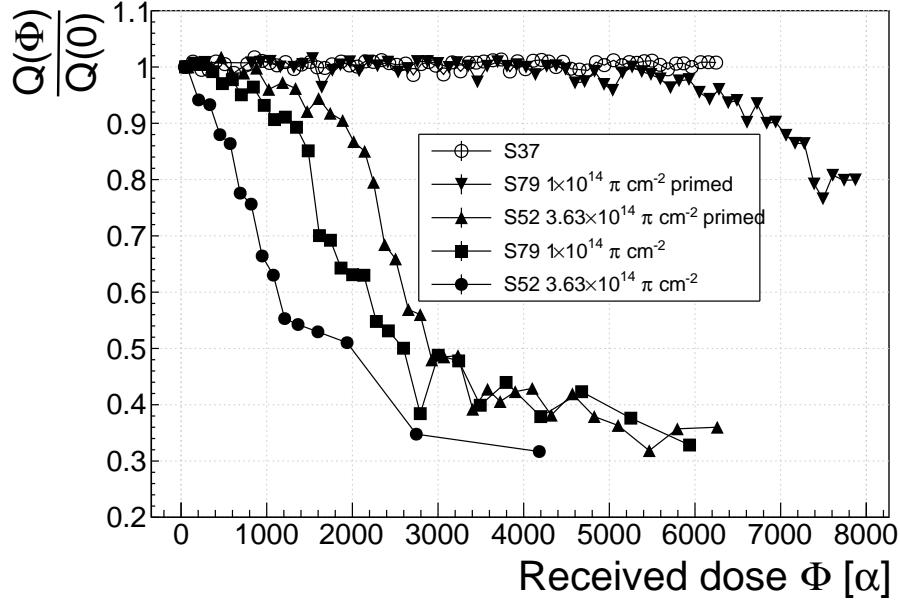


Figure 1.9: A relative drop in charge collection efficiency as a function of the received  $\alpha$  dose for non-irradiated and irradiated diamond samples.

364 collection efficiency using the CIVIDEC Cx spectroscopic amplifier. The charge col-  
 365 lected at every measurement point  $Q(\Phi)$  is compared to collected charge of the first  
 366 measurement  $Q(0)$ . The resulting ratio  $\frac{Q(\Phi)}{Q(0)}$  for all samples is shown in figure 1.9.  
 367 Each measurement point is an average of 30 consecutive  $\alpha$  hits. The conclusions  
 368 drawn are the following:

- 369 -  $Q(\Phi)$  for the non-irradiated S37 is stable as compared to  $Q(0)$  over the course  
 370 of the measurement.
- 371 - The initial efficiency of the irradiated S52 and S79 starts decreasing already at  
 372 a low  $\alpha$  count.
- 373 - The charge collection efficiency of the unprimed irradiated samples drops much  
 374 faster than after priming.
- 375 - The particle count rate decreases with decreased efficiency, which is clearly seen  
 376 in the unprimed S52 data where the data points at a low efficiency are much  
 377 further apart.

378 The absolute values are not shown here because only the relative drop is of interest  
 379 in the scope of the long-term stability tests.

380 To investigate this sudden drop in efficiency, the current pulse shapes using a  
 381 CIVIDEC C2 current amplifier have to be observed, as shown in figure 1.10. The  
 382 shape of the pulse holds more information about the charge carrier properties in the  
 383 sensor than solely the value of the integrated charge. This time only the primed

### 1.3. RADIATION LIMITATIONS

---

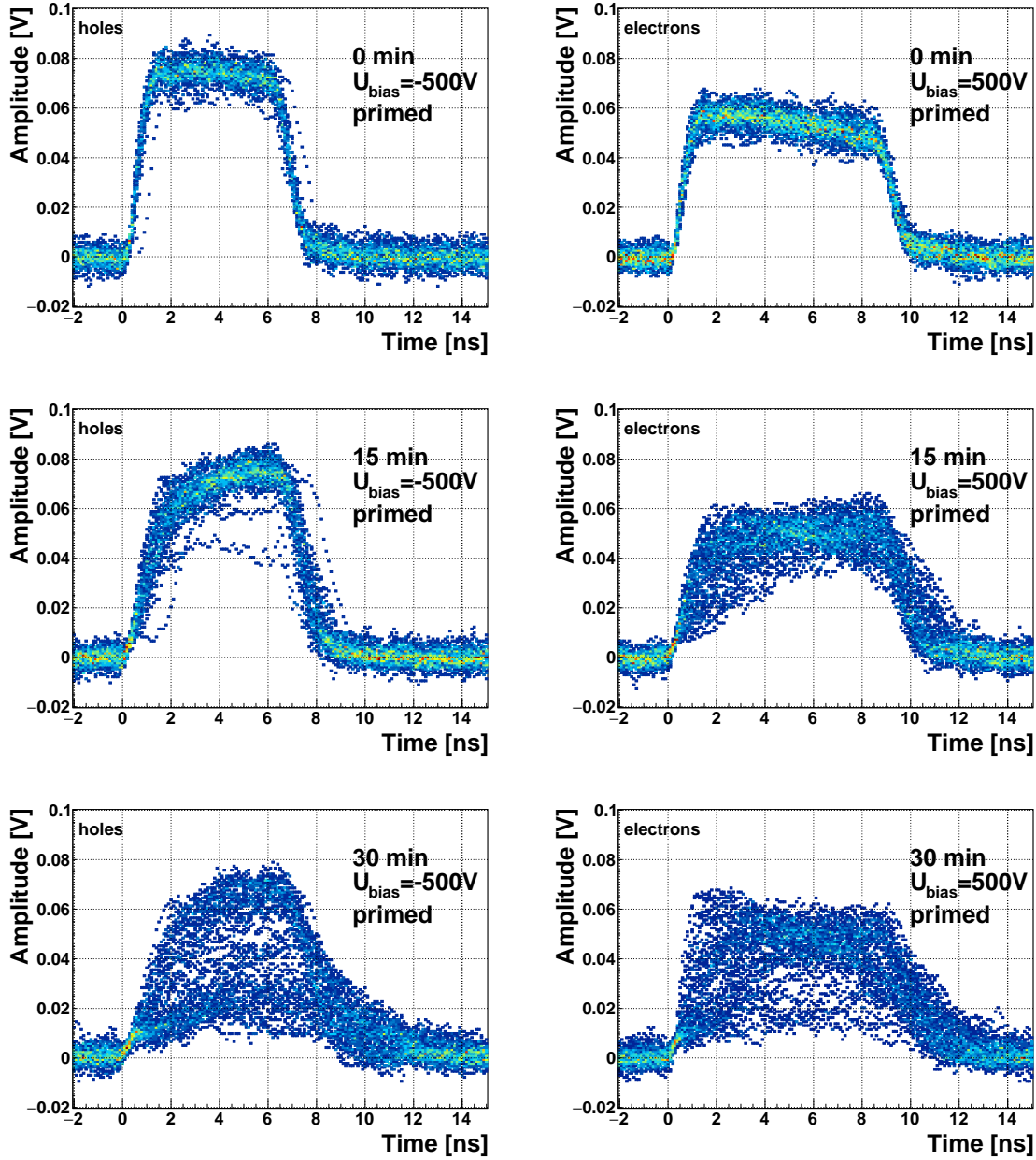


Figure 1.10: The signal of the irradiated and primed S79 deteriorates with time for both polarities. Every plot contains 60 superimposed pulses.

384 S79 sample has been tested. Both the hole and the electron collection are observed  
 385 to determine whether they behave differently or not. The raw acquired data in fig-  
 386 ures 1.10 show that the initially stable pulses start deteriorating; suddenly several  
 387 different shapes start appearing, some still very similar to those from the beginning  
 388 while the others with almost zero amplitude.

389 A more dedicated analysis of the first observation has been carried out as follows:  
 390 at the beginning of the test when the diamond is still operating stably, 60 pulses are

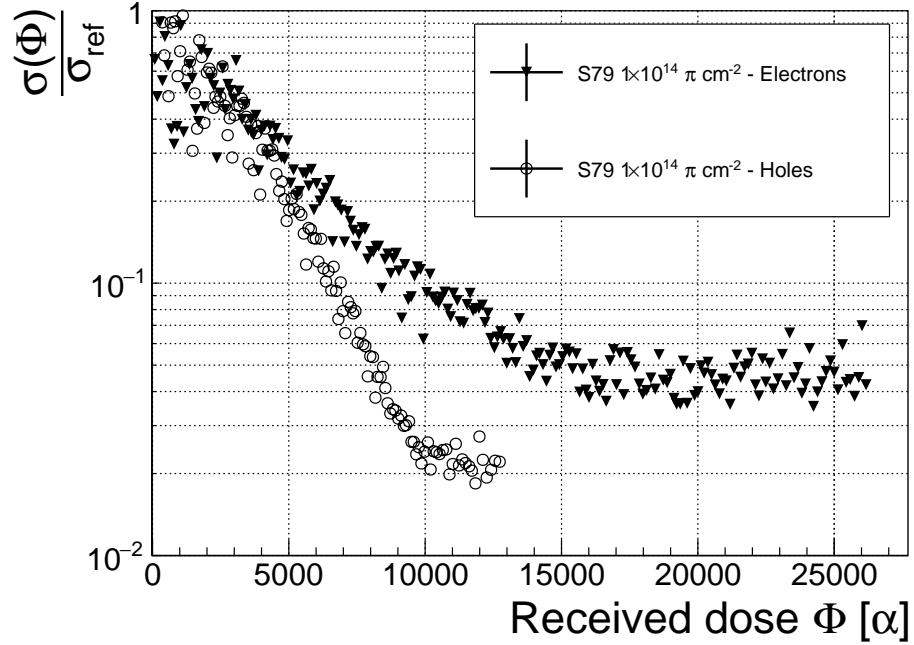


Figure 1.11: Deterioration of the pulse shapes with time.

recorded. An average pulse is calculated. This is a reference pulse for the subsequent measurement points. Then an RMS of the individual pulses  $\sigma_n$  with respect to the reference pulse is calculated and the resulting RMS values are summed together into  $\sigma_{\text{ref}}$ :

$$\sigma_{\text{ref}} = \sum_{n=1}^{60} \sigma_n. \quad (1.9)$$

All the subsequent data points also consist of a set of 60 pulses. At every data point the summation of the RMS values of the individual pulses with respect to the initial averaged pulse  $\sigma$  is calculated according to equation 1.9. The ratio between the initial  $\sigma_{\text{ref}}$  and discrete values  $\sigma$  gives a measure of the change of the pulse shape with respect to the reference pulse at the start of the measurement. Therefore the initial value is 1 and it decreases if the RMS values of subsequent data points are higher. Figure 1.11 shows the ratio  $\frac{\sigma_{\text{ref}}}{\sigma(\alpha \text{ dose})}$ . From the data obtained it can be concluded that the initial pulse shape quickly starts deteriorating. In fact, the deterioration of the shape follows an approximate exponential decay function, which can be fitted to the data. The resulting decay constants for electrons and holes are  $\tau_e = (4400 \pm 150) \alpha^{-1}$  and  $\tau_h = (3300 \pm 140) \alpha^{-1}$ . The electrons retain the initial shape for longer. The deteriorated shapes also seem to be for a factor of 2 better than those of the holes.

**Discussion** One hypothesis is that this behaviour is caused by space-charge. Some moving charges get stopped in the charge traps in the bulk for a long time, building up regions of space-charge. The built up space-charge affects the electric field, making

### 1.3. RADIATION LIMITATIONS

---

410 it non-uniform. The non-uniform field in turn affects the drifting charge carriers,  
 411 slowing them down or speeding them up, depending on the field gradient. Since the  
 412 movement of the carriers is inducing the electric current, the field gradient can be  
 413 observed in the current signal.

414 **Restoring the pulse shapes** Finally, an effort has been made to find a way for the  
 415 pulse shapes to return to their initial state. Five methods are listed:

- 416 1. Removing the source and leaving the bias voltage switched on,
- 417 2. Removing the source and switching the bias voltage off,
- 418 3. Priming with  $\gamma$  at a rate of  $400 \text{ s}^{-1}\text{cm}^{-1}$  without applied bias voltage,
- 419 4. Priming with  $\beta$  at a rate of  $1000 \text{ s}^{-1}\text{cm}^{-1}$  with applied bias voltage and
- 420 5. Priming with  $\beta$  at a rate of  $1000 \text{ s}^{-1}\text{cm}^{-1}$  without applied bias voltage.

421 Before starting each method, the diamond sample S79 is first primed using a  $^{90}\text{Sr}$   
 422 source for approximately one hour. Then the bias voltage is switched on and an  
 423  $^{241}\text{Am}$  source is put on top. The pulses produced by the incident  $\alpha$  particles have a  
 424 proper rectangular pulse at the beginning, but then start changing – first gradually  
 425 and later increasingly more in an erratic way, as described in the text above. After  
 426 approximately 30 minutes, one of the methods is tested. When a “healing” procedure  
 427 is started, a set of 60 pulses is taken at irregular points of time to observe the change  
 428 in the pulse shape and to assess the quality of the “healing” procedure. Then the  
 429 bias voltage is switched off and the sample is primed again to reset its state before  
 430 starting with the next run.

431 The results depicted in figure 1.12 show that the methods (3) and (5) improve the  
 432 shape, method (2) helps slowly, (1) does not show any change with time and (4) at first  
 433 improves, but then significantly degrades the shape. The effect observed in method  
 434 (4) has already been described in [15]. The “healing” process therefore depends on  
 435 the rate of radiation, the bias voltage and the time of exposure. The ionising radiation  
 436 creates free charges, which quickly recombine close to the place of generation. It is  
 437 likely that they also release the charges trapped during the measurement, reducing the  
 438 overall effect of the space-charge. The traps get filled with both flavours of carriers,  
 439 thus they are neutralised. The pulse shape gradually returns to its initial state.

Procedure	Source	Type of radiation	Bias voltage	Effectiveness
1	/	/	ON	no
2	/	/	/	slow
3	$^{60}\text{Co}$	$\gamma$	/	YES
4	$^{90}\text{Sr}$	$\beta$	ON	no
5	$^{90}\text{Sr}$	$\beta$	/	YES

441 Table 1.2: Effectiveness of healing procedures.

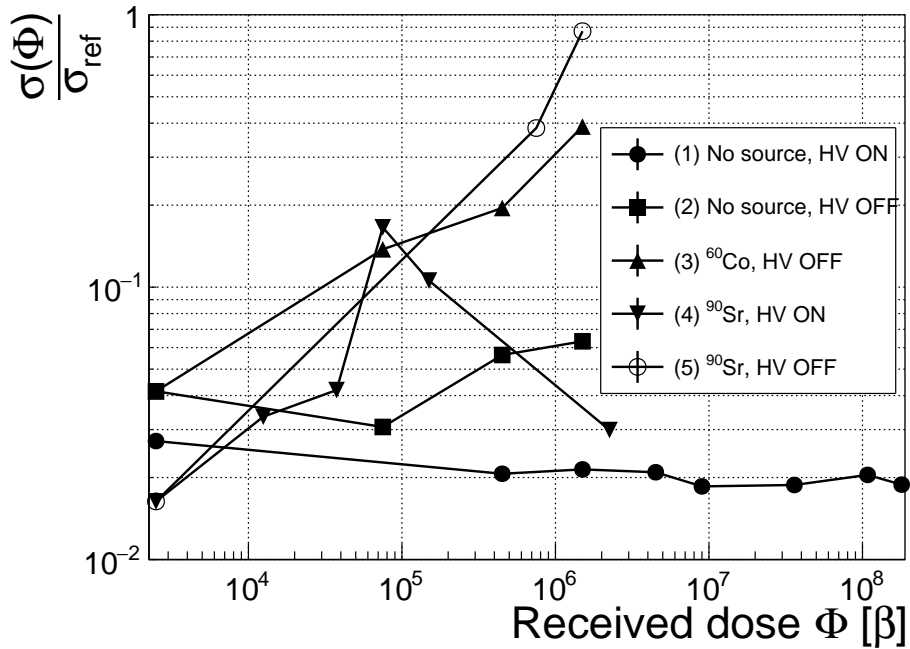


Figure 1.12: Comparison of the five procedures for the “healing” process for an irradiated diamond that had been exposed to  $\alpha$  radiation with a rate of  $10^1 \text{ s}^{-1}$ , with the bias voltage switched on, for at least 30 minutes.

In summary, the shape of the pulses caused by  $\alpha$  radiation changes with time for irradiated samples. The shape of the pulses gets distorted and becomes erratic. Charge collection decreases and its spread increases. This happens even faster for non-primed diamonds. To “heal” the diamond – to bring the pulse shapes back to their initial shape – the sample must be primed using a  $\beta$  or a  $\gamma$  source for several minutes without bias voltage. Switching to the inverse polarity for a few seconds helps a bit, but in a long run distorts the signal, which cannot return to its initial shape.

450 **1.4 Temperature limitations**

451 A test has been carried out to evaluate the effect of temperature changes on the  
452 output signal of the diamond sensors. A cryostat filled with liquid helium is used to  
453 cool down the sensor during the measurement process. The current signal response  
454 to  $\alpha$ -particles is measured at 18 temperature points between 4 K and 295 K. At  
455 every temperature point a set of 300 pulses is recorded at various bias voltages. The  
456 resulting data show that the charge collection is stable from RT down to 150 K where  
457 it starts decreasing. It stabilises again at about one third of the initial value at 75 K.  
458 This behaviour was first measured and discussed by H. Jansen [13].

459 The band gap energy in diamond is equal to  $E_g = 5.5$  eV while the average energy  
460 to produce an electron-hole pair is  $E_{e-h} = 13.25$  eV. This means there is excessive  
461 energy deposited in the diamond bulk. The incident  $\alpha$ -particle stops within  $\sim 10\text{--}15$   $\mu\text{m}$  of the bulk,  
462 transferring all its energy to the lattice during deceleration. A part of this energy directly ionises the carbon atoms, creating free electron-hole pairs.

463 The remaining energy, however, is converted into lattice vibrations – phonons [20,  
464 13]. In other words, the lattice within the ionisation volume (approximately  $\sim 15 \mu\text{m} \times \sim 2 \text{ nm}$   
465 in size) is briefly heated up. The hot plasma then cools down to the temperature of  
466 the surrounding material by means of heat dissipation, i.e. phonon transport.

467 The free electron binds with the free hole into a bound state (not recombination)  
468 – the exciton [16]. The exciton binding energy is 80 meV, which introduces an energy  
469 level within the forbidden gap just under the conduction band. At higher temper-  
470 atures the lattice provides enough energy to thermally excite the electron from the  
471 exciton state back to the conduction band. At lower temperatures, however, the ex-  
472 citon lifetime increases, which means that it takes a longer time for the electrons to  
473 get re-excited to the conduction band. The re-excitation lifetime at room temper-  
474 ature is  $\sim 30$  ps, increasing to  $\sim 150 \mu\text{s}$  at 50 K [13]. This means that some of the  
475 bound electrons do not even start drifting within the period of  $\sim 10$  ns, which is the  
476 expected carrier drift time. When they are finally freed, the current they induce is  
477 already hidden in the electronics noise. The effective area of the observed current  
478 pulse is therefore smaller than that of a pulse induced by all the carriers drifting at  
479 the same time. This in effect reduces the measured collected charge. The longer the  
480 time constant, the lower the measured collected charge, as shown in section 1.4.2.

482 **1.4.1 Temperature-variant  $\alpha$ -TCT before irradiation**

483 Three sCVD diamond samples have been tested at a range of temperatures using  
484 the  $\alpha$ -TCT technique. At each temperature point, the bias voltage is set to several  
485 positive and negative values. A set of 300 pulses is recorded at every data point  
486 and averaged offline. The resulting averaged pulses of sample S37 at the 260 K  
487 temperature point and a bias voltage of  $\pm 700$  V,  $\pm 500$  V and  $\pm 400$  V are shown in  
488 figure 1.13. The pulses induced by holes as charge carriers are shorter than those  
489 induced by electrons, which means that holes travel faster in diamond. The area of

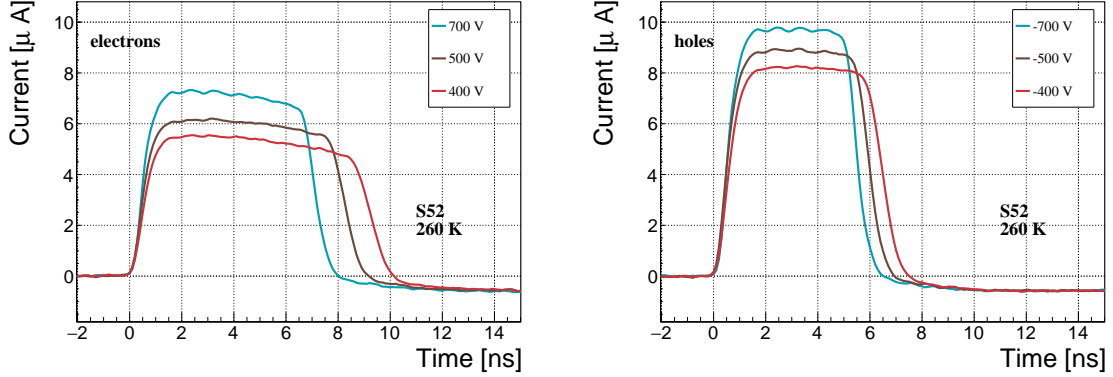


Figure 1.13: Varied bias voltage at a fixed temperature.

the pulse, however, is the same for both polarities, which corresponds to the fact that the same amount of charges is drifting in both cases.

Figure 1.14 shows pulses at a bias voltage set to  $\pm 500$  V across the range of temperatures between 4 K and 295 K. Several conclusions can be drawn by observing their shape. First, the pulse shapes change with decreasing temperature. The pulse time gets shorter and higher, hinting at the faster carrier drift velocity  $v_{\text{drift}}$ . Second, between 150 K and 75 K there is a significant change in shape - the time constant of the rising edge increases significantly and the pulse area decreases. From 75 K down to 4 K there is no significant change. Last, the top of the pulse at the S52 is not flat, which means that a portion of the drifting charge is lost along the way. This is due to charge trapping, likely by means of crystal defects or impurities.

#### 1.4.2 Temperature-variant $\alpha$ -TCT after irradiation

The irradiated S79 and S52 have been re-tested in the cryostat after irradiation. The aim is to observe how their pulse shapes change with decreasing temperature, in particular the decaying top of the pulses, as shown in figure 1.15. The decay time gives information on trapping of charge carriers while travelling through the diamond bulk. A variation of the decay time constant as a function of temperature might help to reveal the type and depth of the charge traps. To observe these effects or lack thereof, a number of requirements have to be met. First, the diamond samples are intentionally not primed prior to the experiment because priming would improve the pulse shapes and possibly change the decay time constant of the signal. Second, keeping in mind that the pulse shape of irradiated diamonds changes with time, the duration of the measurement of an individual data point has to be short – of the order of 30 seconds. Last, the sequence of the bias voltage settings is important, the reason for which is explained below.

Unfortunately it is not possible to avoid temporal pulse changes. For instance, one measurement point takes approximately one minute. After the measurement, the bias voltage polarity is swapped for a few seconds to bring the diamond back into

#### 1.4. TEMPERATURE LIMITATIONS

---

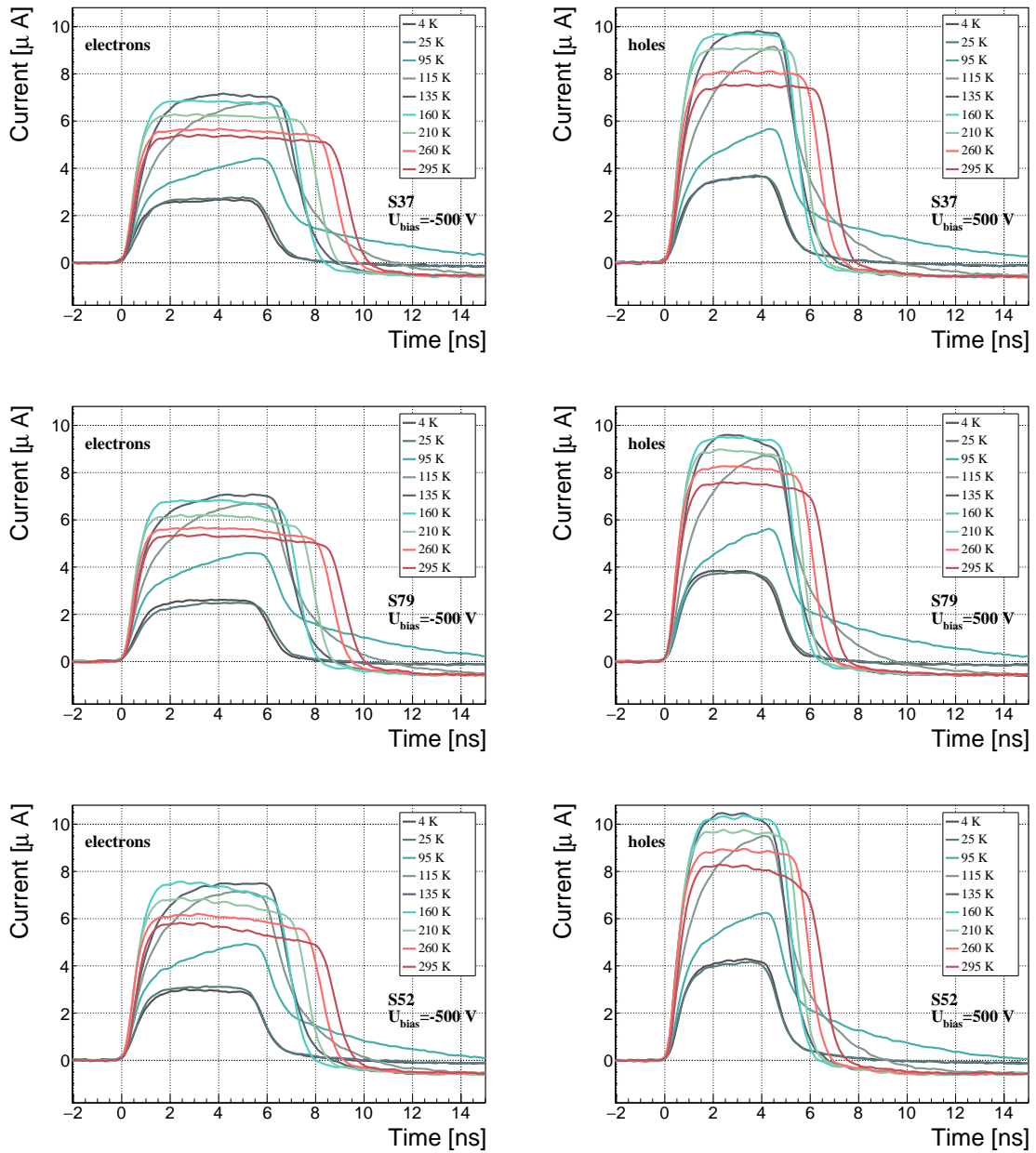


Figure 1.14: Several data points between 4 K and 295 K at a bias voltage of  $\pm 500$  V.

its initial state. But a few seconds with respect to a minute are not enough, but due to time constraints this cannot be avoided. Therefore when the bias voltage is set to the next value, there is still some residual effect of the previous measurement. Similar to the effects of polarisation, this effect is also decreasing the pulse height. This can be observed in figure 1.15, which shows the resulting pulses of S52 for bias voltages of  $\pm 200$  V,  $\pm 300$  V,  $\pm 400$  V and  $\pm 500$  V at 230 K and 260 K. In this case the measurement sequence is: 230K (200 V, 300 V, 400 V, 500 V, -500 V, -400 V, -300 V), 260 K (-200 V, -300 V, -400 V, -500 V, 500 V, 400 V, 300 V). The changes in pulse shapes for holes at 230 K and 260 K cannot be attributed to the temperature change. Instead, the explanation could lie in diamond “polarisation”. This means that, when exposed to an electric field with  $\alpha$  measurements ongoing, an internal electric field of inverse polarity builds up in the diamond, which effectively reduces the overall electric field. This internal field does not dissipate when the external bias voltage is switched off. The diamond becomes “polarised”. When switching the polarity of the external bias voltage, the internal and external electric field point in the same direction at the beginning, increasing the overall electric field and with it the pulse height. In figure 1.15 this happens when switching from 500 V (figure 1.15a) to -500 V (figure 1.15b) at 230 K. The built up polarisation contributes to the pulse having a sharp rising edge and a high amplitude. This effect decays during the next two voltage points. There would be a handful of ways to avoid this polarisation effect in the data:

1. After every data point invert the bias voltage and leave it to return to a neutral state for the same amount of time,
2. Make a hysteresis of data points, going from minimum negative to maximum positive bias several times,
3. Reduce the measurement time at every bias voltage setting.

Unfortunately, options (1) and (2) are very time consuming and would increase the overall experiment time to over one day. The third option would worsen the resulting averaged pulses. In the end an alternative option has been chosen: alternating the starting bias voltage and the sequence at every temperature point. With this option, a meaningful systematic error in analysing the pulse shapes can be attained.

Figure 1.16 shows the irradiated S52 and S79 as well as the non-irradiated S37 for comparison, all at a bias voltage of  $\pm 500$  V and at several temperature points between 4 K and 295 K. It is evident that the radiation damage affects the shape of the pulses across all temperatures.

### 553 Collected charge as a function of temperature

554 The area below the current pulse is proportional to the charge collected by the dia-  
555 mond detector. The collected charge is measured as a function of temperature. First,  
556 the amplitude values of the averaged pulses at a bias voltage of  $\pm 500$  V and across

## 1.4. TEMPERATURE LIMITATIONS

---

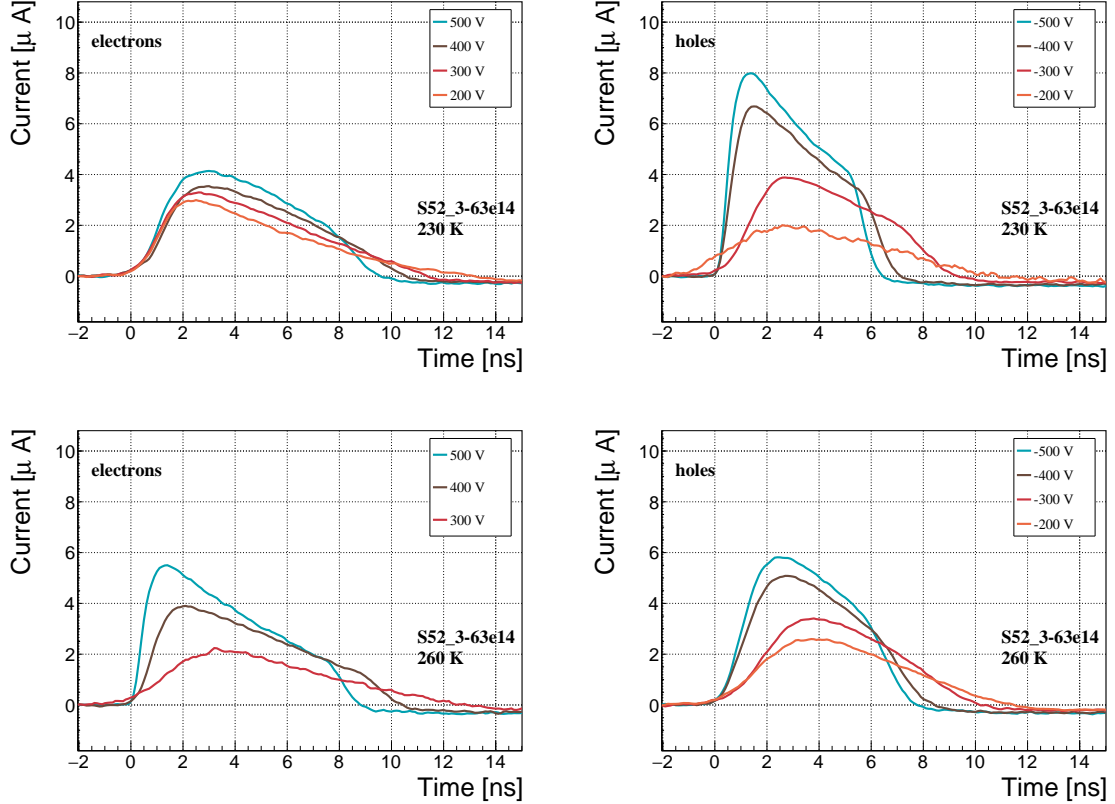


Figure 1.15: Varied bias voltage at a fixed temperature for an irradiated sample.

the temperature range between 4 K and 295 K have to be integrated. Then a calibration factor is used to derive the charge for all data points. This factor is obtained using a Cx charge-sensitive amplifier. The resulting values for electrons and holes are plotted in figures 1.17 and 1.18, respectively. The drop in collected charge and a first model is given in [13]. In the framework of this thesis the focus is on the effect in the irradiated devices. The new contribution are the data points for the irradiated samples. The values for all samples are fairly stable in the range between 4 K and 75 K and between 150 K and 295 K. However, in the values for the irradiated S52 some excursions can be observed. This is due to the sequence of the measurement steps, which results in a hysteresis effect explained in the preceding text.

The collected charge drops significantly from 150 K down to 75 K. In the non-irradiated samples the values in the lower temperature range are approximately 30 % of the values in the high range. For the irradiated samples this difference is lower – 35 % for S79 and 50 % for S52.

An interesting detail in figure 1.17 is that the ratio between the values for non-irradiated samples and their irradiated counterparts at the lower temperature range is different than at the higher range. In other words, the charge loss due to irradiation damage is lower for temperatures between 4 K in 75 K than for temperatures between 150 K and 295 K. The irradiated S52 collects 78 % of the initial charge in the low

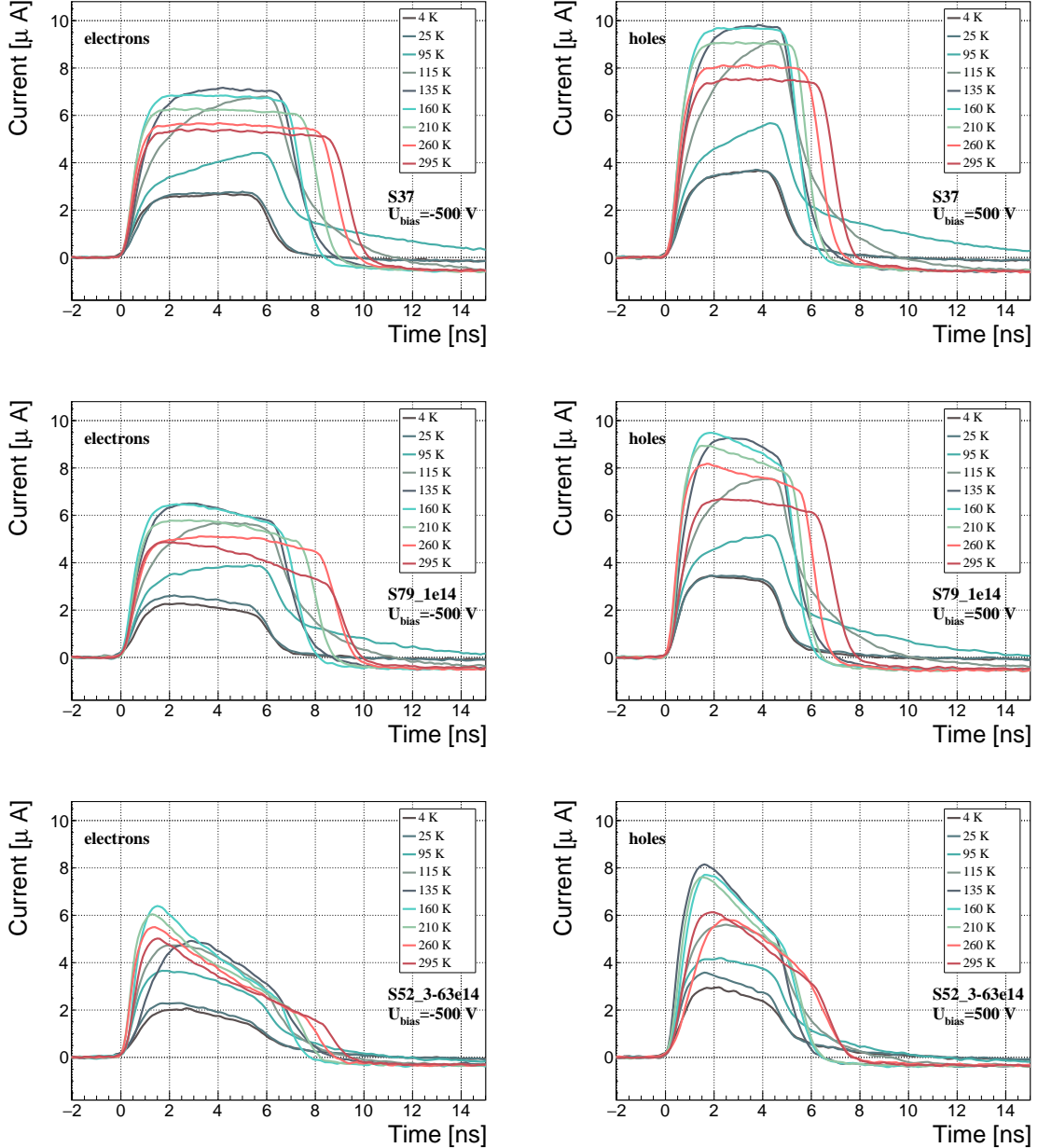


Figure 1.16: After irradiation: several data points between 4 K and 295 K at a bias voltage of  $\pm 500$  V.

temperature range, but only 59 % of the initial charge for the high range. The values for S79 for these two temperature ranges are 100 % and 90 %, which means that the drop in charge collection efficiency after irradiation to  $1 \times 10^{14} \pi \text{ cm}^{-2}$  is negligible for temperatures below 75 K.

#### 1.4. TEMPERATURE LIMITATIONS

---

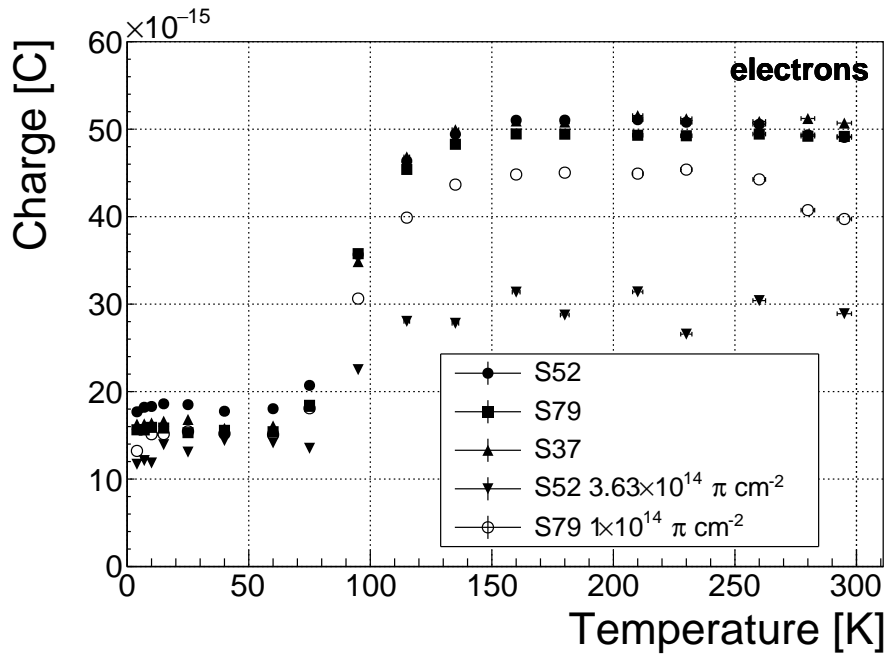


Figure 1.17: Collected charge for electrons as a function of temperature.

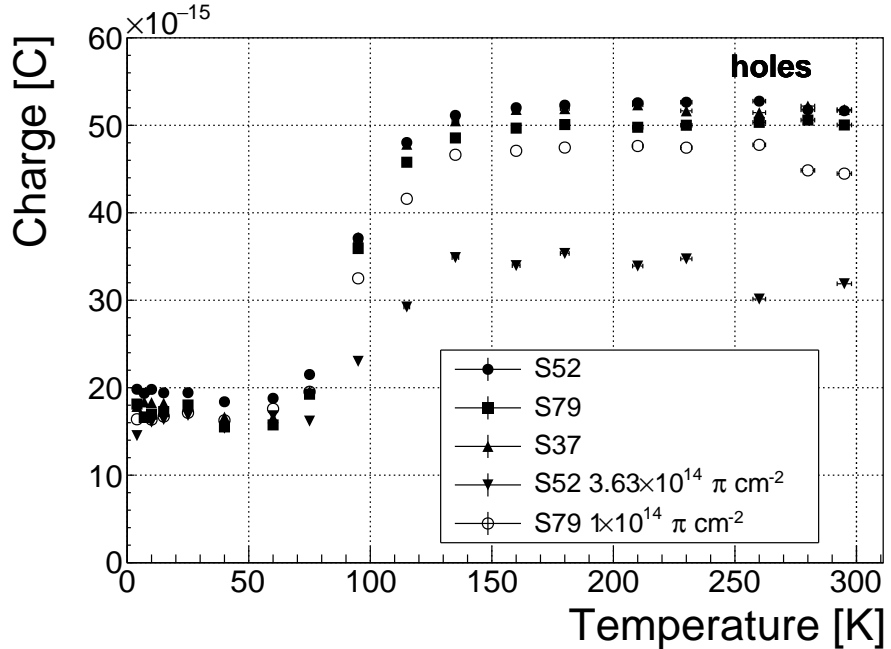


Figure 1.18: Collected charge for holes as a function of temperature.

#### 580 Charge trapping

581 The charge carriers that drift through the bulk get stopped in the charge traps with  
 582 a certain probability. This trapping happens uniformly throughout the diamond. In  
 583 other words, the number of carriers in the moving charge cloud is gradually reduced.

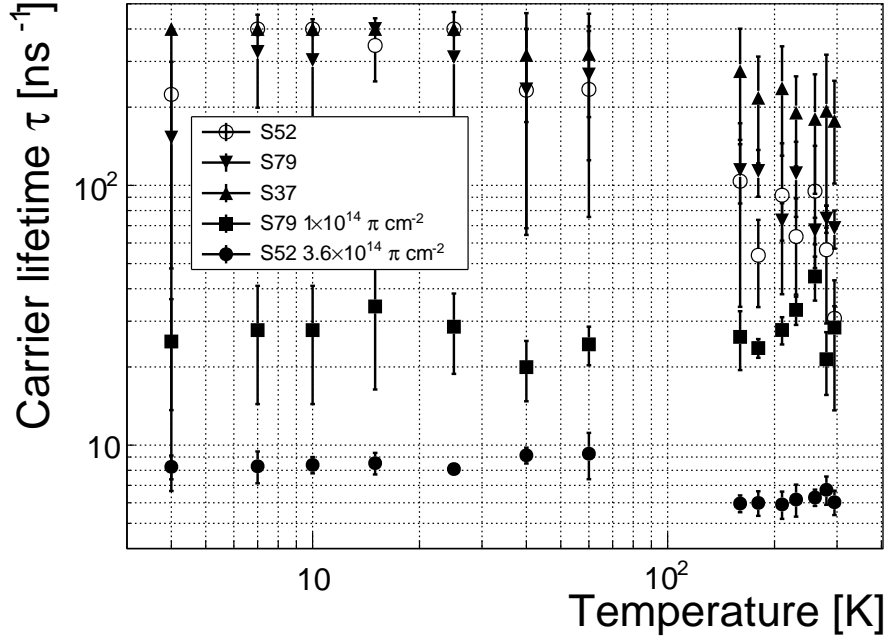


Figure 1.19: This figure shows the charge carrier lifetime as a function of temperature. The data points between 75 K and 150 K are omitted. The fit function only works well on signals with a well pronounced decaying top.

- 584 This in turn reduces the induced current. The function for the number of drifting  
 585 carriers per unit of length is a decaying exponential function:

$$I(t) = I_0 + I(0) \cdot e^{-\frac{t-t_0}{\tau}}, \quad (1.10)$$

586 where  $I(0)$  is the initial induced current,  $I_0$  is the end current,  $t$  is time,  $t_0$  is temporal  
 587 displacement of the pulse and  $\tau$  is the decay time constant. This value describes how  
 588 long it takes before the amplitude of the pulse decreases to 63 % of its initial height.

589 The decaying exponential function is fitted to the decaying top of the averaged  
 590 pulses at a bias voltages of  $\pm 400$  V and  $\pm 500$  V across all temperatures excluding  
 591 the transitional range between 75 K and 150 K. The resulting decay time constants  
 592  $\tau$  for an individual temperature point are not equal, which stems from the fact that  
 593 the pulses change with time due to “polarisation”. This counts as a systematic error.  
 594 Therefore the fitted  $\tau$  for  $\pm 400$  V and  $\pm 500$  V are averaged into one value representing  
 595 the measurement at that temperature point. Figure 1.19 shows the fitted  $\tau$  for the  
 596 five samples between 4 K and 295 K. In principle the time constants should be infinite  
 597 for a perfect and non-irradiated sample. Here a slightly tilted top of the pulse due to  
 598 space-charge is already successfully fitted with an exponential function (a pitfall in an  
 599 automatic analysis), resulting in a  $\tau$  of the order of  $(200 \pm 20) \times 10^{-9}$  s. Consequently  
 600 the fitting method is not adequate for non-irradiated samples. For the irradiated  
 601 samples the fit becomes increasingly more meaningful. As seen in figure 1.19, the  
 602 fitted values of the irradiated samples are fairly stable across all temperatures. There

## 1.4. TEMPERATURE LIMITATIONS

---

is a slight increase in the decay time constant of the S52 from  $(6.0 \pm 0.5) \times 10^{-9}$  s above 150 K to  $(8.5 \pm 0.9) \times 10^{-9}$  s below 75 K. On the other hand, this step is not observable in the S79 data. With only one sample exhibiting this behaviour, the effect is not significant enough. Judging by the data acquired, the samples would need to be irradiated to doses above  $1 \times 10^{14} \pi \text{ cm}^{-2}$  to quantify this effect in detail. So far this effect is not regarded as significant for the scope of this thesis. Building on this assumption, the conclusion is that the signal decay time constant for irradiated sCVD diamond is constant across the temperature range between 4 K and 295 K, excluding the transitional range between 75 K and 150 K where it cannot be quantified properly.

Taking into account the discussion above, all the values can be averaged into one decay constant. Figure 1.20 shows these values for all samples as a function of the received  $\pi_{300 \text{ MeV}}$  radiation dose. To estimate the charge carrier lifetime with respect to the radiation dose received, a similar model is used than that in section 1.5. This model states that the charge carrier lifetime is linearly decreasing with increasing radiation dose:

$$\frac{1}{\tau} = \frac{1}{\tau_0} + \kappa_\tau \cdot \Phi \quad (1.11)$$

$$\tau = \frac{\tau_0}{\kappa_\tau \tau_0 \Phi + 1} \quad (1.12)$$

where  $\tau_0$  is the lifetime for a non-irradiated sample (real lifetime, therefore of the order of 400 ns),  $\tau$  is the lifetime of an irradiated sample,  $\Phi$  is the received radiation dose and  $\kappa_\tau$  the lifetime degradation factor. For these data the fitted factor is equal to  $\kappa_\tau = (3.5 \pm 0.8) \times 10^{-16} \text{ s cm}^2 \pi_{300 \text{ MeV}}^{-1}$ . Using this factor, the steepness of the decay in the pulse shape as a function radiation dose can be estimated. This is highly useful information when designing a system where the current pulse shape is an important factor.

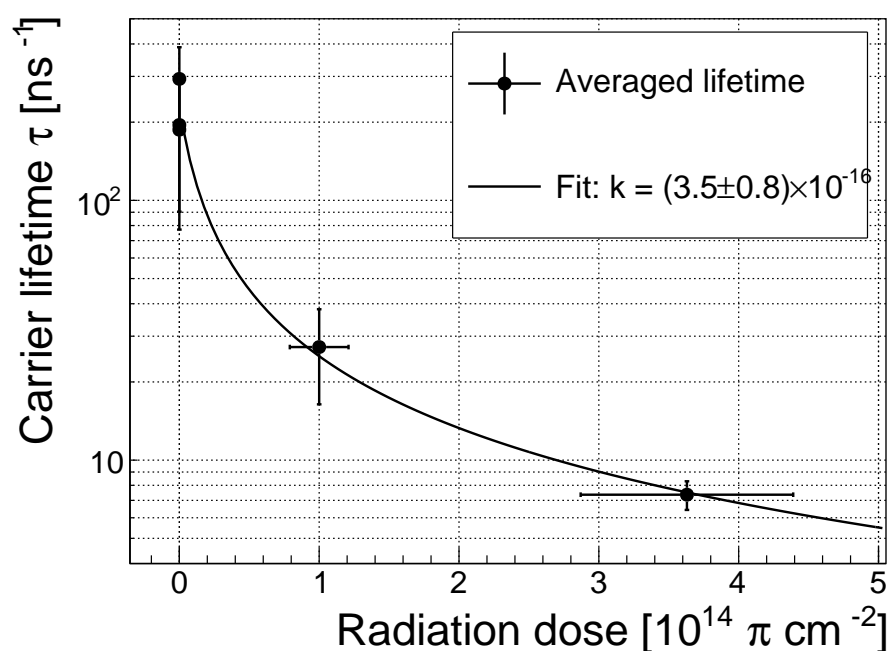


Figure 1.20: This figure shows the carrier lifetime averaged over all temperatures and plotted as a function of the  $\pi$  irradiation dose.

**626 1.5 Conclusion**

627 This chapter gives an overview of the capabilities and limitations of diamond as a  
628 particle detector. Two effects on diamond are studied – radiation and temperature.

629 Two sCVD diamond detectors were irradiated with 300 MeV pions. They were  
630 tested alongside a non-irradiated sample to observe the changes in the ability to detect  
631  $\alpha$ ,  $\beta$  and  $\gamma$  radiation. Their charge collection efficiency was measured in a test beam  
632 facility. The results were compared to the results from the RD42 collaboration and  
633 a DPA model. A radiation damage factor  $k_\lambda = (4.4 \pm 1.2) \times 10^{-18} \mu\text{m}^{-1} \text{cm}^{-2}$  was  
634 obtained for  $\pi_{300 \text{ MeV}}$  particles. The data point was not in agreement with the data  
635 provided by RD42 nor with the model. However, the irradiation process and the low  
636 number of tested samples hold a relatively high statistical uncertainty. In addition,  
637 there was no diamond surface treatment done in between the measurements, as is  
638 the case in the study conducted by RD42. The results obtained in the course of  
639 these measurements are going to be fed into the existing pool of data in the RD42  
640 collaboration.

641 The next step was to test the long-term capabilities for  $\alpha$  detection. The shape  
642 of the ionisation profile was investigated to determine the behaviour of the charge  
643 carriers in the irradiated diamond. An exponential decay was observed in the pulses  
644 of irradiated samples, proving that there are charge traps in the bulk that were created  
645 during irradiation. Then a long-term stability test was carried out. The results show  
646 that the irradiated diamond detectors do not provide a stable and reliable long-term  
647 measurement of  $\alpha$  particles. This might be due to a space-charge build-up in the  
648 bulk, which changes the electric field, affecting the charge carriers. A procedure to  
649 improve the pulse shape using  $\beta$  and  $\gamma$  radiation was proposed.

650 Finally, the diamond sensors were cooled down to temperatures between 4 K and  
651 295 K. Their response to  $\alpha$  particles was observed. The results of the non-irradiated  
652 and irradiated samples were compared. The effect of reduction for the number of  
653 drifting charges due to exciton recombination was observed in both sets of data.  
654 The second set had a superimposed effect of charge trapping during the drift, which  
655 was represented by an exponential decay in the signal. The decay time constant  
656 did not change with temperature. Therefore all temperature points for individual  
657 samples were averaged and the decay time constants were plotted against the received  
658 radiation dose. A lifetime degradation factor  $\kappa_\tau = (3.5 \pm 0.8) \times 10^{-16} \text{ s cm}^2 \pi_{300 \text{ MeV}}^{-1}$   
659 for non-primed diamonds was defined.

# <sup>660</sup> Bibliography

- <sup>661</sup> [1] *DRS4*. <https://www.psi.ch/drs/evaluation-board>.
- <sup>662</sup> [2] *Element Six*. <http://www.e6.com>.
- <sup>663</sup> [3] *IHa Technologies Pte. Ltd.* <https://www.2atechnologies.com>.
- <sup>664</sup> [4] *Paul Scherrer Institute*. <https://www.psi.ch/>.
- <sup>665</sup> [5] *RD42 collaboration*. <http://rd42.web.cern.ch/rd42/>.
- <sup>666</sup> [6] *Determination of operational dose equivalent quantities for neutrons*. ICRU,  
<sup>667</sup> Washington, DC, 2001.
- <sup>668</sup> [7] H. Bethe and J. Ashkin. *Experimental Nuclear Physics*, ed. E. Segre, page 253,  
<sup>669</sup> 1953.
- <sup>670</sup> [8] Giorgio Brianti. SPS North Experimental Area. Technical Report CERN-SPSC-  
<sup>671</sup> T-73-8. LabII-EA-Note-73-4, CERN, Geneva, 1973.
- <sup>672</sup> [9] P. Carazzetti and H. R. Shea. *Electrical breakdown at low pressure for planar  
673 microelectromechanical systems with 10- to 500  $\mu\text{m}$  gaps*. *J. Micro/Nanolith.  
MEMS MOEMS*, (8(3), 031305), Jul-Sep 2009.
- <sup>675</sup> [10] E. Griesmayer and B. Dehning. Diamonds for beam instrumentation. *Physics  
676 Procedia*, 37:1997 – 2004, 2012. Proceedings of the 2nd International Conference  
677 on Technology and Instrumentation in Particle Physics (TIPP 2011).
- <sup>678</sup> [11] Moritz Guthoff, Wim de Boer, and Steffen Mller. Simulation of beam induced  
679 lattice defects of diamond detectors using {FLUKA}. *Nuclear Instruments and  
680 Methods in Physics Research Section A: Accelerators, Spectrometers, Detectors  
and Associated Equipment*, 735:223 – 228, 2014.
- <sup>682</sup> [12] M. Huhtinen. Simulation of non-ionising energy loss and defect formation in  
683 silicon. *Nuclear Instruments and Methods in Physics Research A*, 491:194–215,  
684 September 2002.
- <sup>685</sup> [13] Hendrik Jansen, Norbert Wermes, and Heinz Pernegger. *Chemical Vapour De-  
686 position Diamond - Charge Carrier Movement at Low Temperatures and Use in*

## BIBLIOGRAPHY

---

- 687        *Time-Critical Applications*. PhD thesis, Bonn U., Sep 2013. Presented 10 Dec  
688        2013.
- 689 [14] Claude A. Klein. Radiation-induced energy levels in silicon. *Journal of Applied  
690        Physics*, 30(8):1222–1231, 1959.
- 691 [15] Gregor Kramberger, V. Cindro, A. Gorisek, I. Mandic, M. Mikuz, and M. Zavr-  
692        tanik. Effects of bias voltage during priming on operation of diamond detectors.  
693        *PoS*, Vertex2012:013, 2013.
- 694 [16] W. Y. Liang. Excitons. *Physics Education*, 5:226–228, July 1970.
- 695 [17] M. Mikuž. *Diamond sensors for high energy radiation and particle detection*.  
696        TIPP, 2011.
- 697 [18] V. Sarin. *Comprehensive Hard Materials*. Elsevier Science, 2014. p. 411.
- 698 [19] M. Červ, P. Sarin, H. Pernegger, P. Vageeswaran, and E. Griesmayer. Diamond  
699        detector for beam profile monitoring in comet experiment at j-parc. *Journal of  
700        Instrumentation*, 10(06):C06016, 2015.
- 701 [20] J. L. Yarnell, J. L. Warren, and R. G. Wenzel. Lattice vibrations in diamond.  
702        *Phys. Rev. Lett.*, 13:13–15, Jul 1964.